The first 3T BioMatrix system

Embrace human nature at 3T

MAGNETOM Vida
with BioMatrix

The increasing number of exams, complexity, and cost-pressure are placing challenges on MRI. 3T MRI needs to better handle patient variability, deliver robust results for all patient types, and become more cost-effective.

MAGNETOM Vida, the first MR scanner with BioMatrix Technology, is equipped to master the challenges facing MRI today. 3T MRI with BioMatrix meets these needs with fewer rescans, predictable patient scheduling and consistent, high-quality personalized exams.

Embrace full 3T performance
with unparalleled magnet and gradient power

Embrace true 3T productivity
with GO technologies

Embrace new 3T clinical capabilities
with Inline Compressed Sensing

healthcare.siemens.co.kr

SIEMENS Healthineers

Original Article

PMP

Progress in Medical Physics 30(4), December 2019
https://doi.org/10.14316/pmp.2019.30.4.139
eISSN 2508-4453

Assessment of the Cerebrospinal Fluid Effect on the Chemical Exchange Saturation Transfer Map Obtained from the Full Z-Spectrum in the Elderly Human Brain

Soonchan Park[1], Joon Jang[2], Jang-Hoon Oh[2], Chang-Woo Ryu[1], Geon-Ho Jahng[1]

[1]*Department of Radiology, Kyung Hee University Hospital at Gangdong, College of Medicine, Kyung Hee University, Seoul,* [2]*Department of Biomedical Engineering, Kyung Hee University, Yongin, Korea*

Received 2 October 2019
Revised 3 November 2019
Accepted 4 November 2019

Corresponding author
Geon-Ho Jahng
(ghjahng@gmail.com)
Tel: 82-2-440-6187
Fax: 82-2-440-6932

Soonchan Park and Joon Jang contributed equally to this work.

Purpose: With neurodegeneration, the signal intensity of the cerebrospinal fluid (CSF) in the brain increases. The objective of this study was to evaluate chemical exchange saturation transfer (CEST) signals with and without the contribution of CSF signals in elderly human brains using two different 3T magnetic resonance imaging (MRI) sequences

Methods: Full CEST signals were acquired in ten subjects (Group I) with a three-dimensional (3D)-segmented gradient-echo echo-planar imaging (EPI) sequence and in ten other subjects (Group II) with a 3D gradient and spin-echo (GRASE) sequence using two different 3T MRI systems. The segmented tissue compartments of gray and white matter were used to mask the CSF signals in the full CEST images. Two sets of magnetization transfer ratio asymmetry (MTR_{asym}) maps were obtained for each offset frequency in each subject with and without masking the CSF signals (masked and unmasked conditions, respectively) and later compared using paired t-tests.

Results: The region-of-interest (ROI)-based analyses showed that the MTR_{asym} values for both the 3D-segmented gradient-echo EPI and 3D GRASE sequences were altered under the masked condition compared with the unmasked condition at several ROIs and offset frequencies.

Conclusions: Depending on the imaging sequence, the MTR_{asym} values can be overestimated for some areas of the elderly human brain when CSF signals are unmasked. Therefore, it is necessary to develop a method to minimize this overestimation in the case of elderly patients.

Keywords: CEST, Cerebrospinal fluid signal, MTR asymmetry, Sequence type, Brain-tissue degeneration

Introduction

Chemical exchange saturation transfer (CEST) imaging is, which is a recently developed MRI contrast approach for imaging molecules and proteins in the body.[1)] The technique helps indirectly detect low-concentration compounds with exchangeable protons via the varying bulk-water proton signal from saturation transfer.[2-4)] The basic principle of CEST MRI involves selectively saturating an exchangeable solute proton that resonates at a frequency different from that of the bulk-water proton by applying a radiofrequency (RF) pulse.[5)] This saturated solute proton is subsequently exchanged with a bulk-water proton, and the solute proton is replaced by a non-saturated water proton, since the number of bulk-water protons is much greater than that of solute protons. This phenomenon slightly reduces the water signal intensity. If the saturation time is sufficiently long, the RF pulse enhances this signal attenu-

ation from the saturation effect, which eventually becomes quantifiable by measuring the decreased water signal, thereby allowing indirect imaging of low-concentration solutes. The frequency-dependent saturation effects are visualized as a signal loss at a specific frequency, known as a Z-spectrum[6] or CEST spectrum. The saturation effects are asymmetric with respect to the water resonance frequency and can be quantified by performing an asymmetry analysis, wherein the water signals from either side of the Z-spectrum are subtracted from each other. A CEST asymmetry map called the magnetization transfer ratio asymmetry (MTR_{asym}) map is generally used to evaluate the CEST effects.

Targeted, endogenously exchangeable, solute protons already exist in molecules within the human body, including amide (–NH), amine ($–NH_2$), guanidine ($[NH_2]_2$), and hydroxyl (–OH) groups, with optimal exchange properties under physiological conditions.[7] Unlike exogenous CEST sources, endogenous CEST sources do not lead to problems associated with injection or toxicity. Moreover, if the properties of certain endogenous CEST sources change in a specific disease state, they can serve as useful imaging biomarkers for the early diagnosis of diseases. For example, amino acids contain amide, amine, guanidine, and/or hydroxyl protons that are constituents of amyloid-beta proteins, which accumulate in the brains of patients with Alzheimer's disease.[8,9] Furthermore, the levels of myo-inositol, which is a metabolite in the brain containing hydroxyl protons, have been reported to be greater in the brains of patients with Alzheimer's than in the brains of healthy control subjects.[10] Thus, CEST MRI can play a key role in investigating brain changes in patients with neurodegenerative diseases. However, brain degeneration results in tissue loss,[11] leading to perivascular spaces, which are usually replaced by cerebrospinal fluid (CSF). Owing to the contribution of the CSF signal, the CEST asymmetry value is usually high near the ventricular area or the perivascular space, because the CSF effects tend to give higher signals particularly near the direct water saturation frequency.[4] Therefore, obtaining accurate CEST effects on the gray and white matter is difficult because of the contribution of CSF in the elderly human brain.[12] No study has investigated the contribution of CSF to CEST signals in the brain of an elderly subject.

The objective of this study, therefore, was to evaluate the CEST asymmetry with and without the contribution of CSF signals in the elderly human brain using two different 3T MRI sequences. We hypothesized that the CEST asymmetry value without masking the CSF signals (unmasked condition) would be greater than that with masking (masked condition).

Materials and Methods

1. Subjects

This study was approved by the ethical committee of the Institutional Review Board of Kyung Hee University Hospital at Gangdong (No. 2015-02-006-001). Written informed consent was obtained by all participants enrolled. Twenty subjects were studied using two different sequences. Ten subjects (Group I) were scanned with a three-dimensional (3D)-segmented gradient-echo echo-planar imaging (EPI) sequence to obtain full Z-spectrum signals using a 3T MRI system (Achieva 3.0T; Philips, Amsterdam, Netherlands). All the subjects were woman. Ten other subjects (Group II) were scanned with a 3D gradient and spin-echo (GRASE) sequence to obtain full Z-spectrum signals using another 3T MRI system (Ingenia 3.0T; Philips). In this group, eight were women and two were men. The subjects were recruited for optimizing the CEST MRI techniques employed in Kyung Hee University Hospital at Gangdong to ultimately apply this technique for imaging the brain of patients with Alzheimer's disease. Table 1 lists the characteristics of the subjects and the CEST signal acquisitions.

2. MRI acquisition

The first full Z-spectrum data were acquired with the 3D-segmented gradient-echo EPI sequence[13] using an eight-channel sensitivity-encoding (SENSE) coil. To induce CEST saturation exchange, we set the B_1 amplitude of the saturation pulse as 1 μT; the saturation pulse duration per pulse as 70 ms; and the total number of shots to the center of the k-space as 126. Therefore, the total saturation length was 8.8 seconds. We obtained the full Z-spectrum via 29

Table 1. Characteristics of subjects and the chemical exchange saturation transfer signal acquisitions

Variables	Group I	Group II
Subjects (n)	10	10
Mean age (y)	72.3±9.82	73.3±7.36
Age range (y)	55–83	59–87
Magnetic field (T)	3.0	3.0
Model of MRI system	Achieva	Ingenia
Sequence name	3D-segmented GE EPI	3D GRASE
Saturation B_1 amplitude (μT)	1	2
Saturation pulse duration (ms)	70	200
Total saturation duration (s)	8.8	0.84
Saturation method	Continuous	Alternative
Full Z-scans (n)	29	37
Scan time (s)	567	509

T, Tesla; MRI, magnetic resonance imaging; 3D, three-dimensional; GE, gradient-echo; EPI, echo-planar imaging; GRASE, gradient and spin-echo.

dynamics at offset frequencies ranging from –6.00 ppm to 6.00 ppm with a continuously increasing frequency interval of 0.43 ppm. The first acquired image was the reference image S_0 obtained at an offset frequency of –40. The imaging parameters were as follows: repetition time (TR)/echo time (TE)=150/7.1 ms; acquisition matrix=112×112; acquisition voxel size=2×2×6.40 mm^3; reconstruction voxel size=0.76×0.76×3.20 mm^3; EPI factor=9; flip angle (FA)=7°; field of view (FOV)=220×220×06 mm^3; SENSE factor=2 for the anterior-posterior direction and 1 for the right-left direction; number of slices=33; and imaging orientation=transverse. The scan time was 567 seconds.

The second full Z-spectrum data were acquired with the 3D GRASE sequence[14] by using a 32-channel SENSE coil. To induce CEST saturation exchange, we set the B_1 amplitude as 2 μT; the saturation pulse duration as 200 ms with a 10-ms interval between the pulses; and the number of saturation pulses as 4. Therefore, the total saturation length was 0.83 seconds. We obtained the full Z-spectrum via 37 dynamics at offset frequencies ranging from –5.00 ppm to 5.00 ppm with an alternatively increased frequency interval of 0.25 ppm at offset frequencies ranging from ±0.25 ppm to ±4.00 ppm and thereafter acquired the images at offset frequencies of ±4.5 ppm and ±5.0 ppm. The first acquired image was the reference image S_0 at –40 ppm, and the second acquired image was taken at an offset of 0 ppm with respect to the direct saturation of water. The imaging parameters were as follows: TR/TE=2200/16 ms; acquisition matrix=104×92; acquisition voxel size=2×2×8 mm^3; reconstruction matrix size=1×1×4 mm^3; FA=90°; SENSE factor=2 for the anterior-posterior direction and 1 for the right-left direction; turbo spin-echo (TSE) factor=23; EPI factor=7; number of slices=23; and imaging orientation=transverse. The scan time was 509 seconds.

Finally, for image registration and brain-tissue segmentation, sagittal structural 3D T1-weighted (T1W) images were acquired with the magnetization-prepared rapid acquisition of the gradient echo sequence with the following parameters: TR=8.1 ms; TE=3.7 ms; FA=8°; FOV=236×236 mm^2; and voxel size=1×1×1 mm^3. In addition, T2-weighted TSE and fluid-attenuated inversion recovery images were acquired to examine any brain malformations.

3. Pre-processing of the full Z-spectrum for CSF signals analysis

The MRI data were analyzed using MATLAB (http://www.mathworks.com) (MathWorks, Natick, MA, USA) and Statistical Parametric Mapping Version 12 (SPM12) (http://www.fil.ion.ucl.ac.uk/spm/) (Wellcome Trust Centre for Neuroimaging, London, UK). Fig. 1 shows the pre-processing steps of the 3D T1W and full Z-spectrum images. First, the 3D T1W and full Z-spectrum images were co-registered. Second, the 3D T1W images were segmented into gray and white matter using the CAT12 toolbox (http://www.neuro.uni-jena.de/cat/) (Structural Brain Mapping Group, Jena, Germany) to obtain brain-tissue compartments. Third, the co-registered full Z-spectrum images for each subject were spatially normalized into a Montreal Neurological Institute (MNI) brain template using the subject's deformation field information obtained from the brain-tissue-segmentation step of the 3D T1W image. Finally, the CSF signal in the full Z-spectrum images was masked using information from the segmented gray- and white-matter tissue compartments to evaluate the full Z-spectrum images while minimizing the contributions of the CSF signals. We only included voxels that had more than 50% gray and white

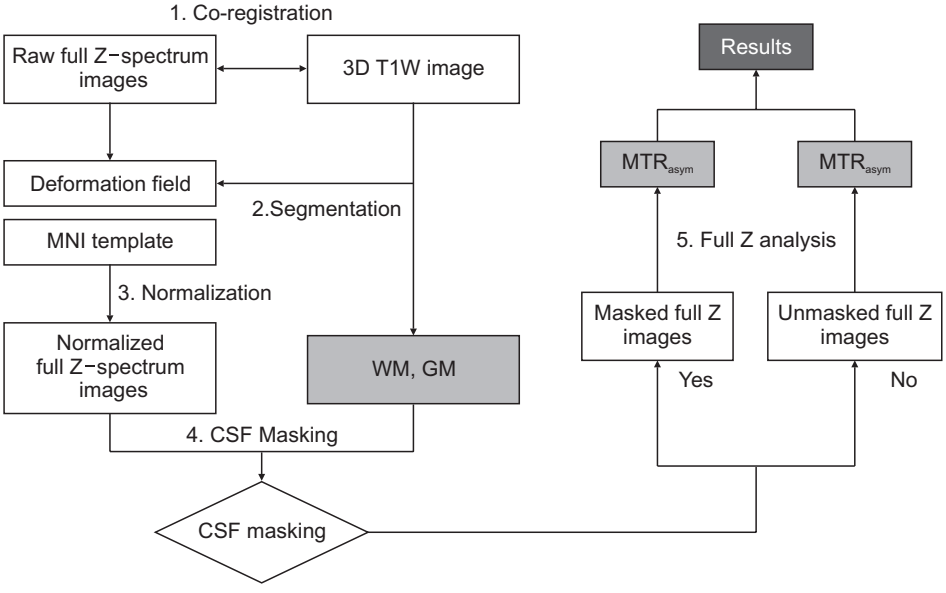

Fig. 1. Processing steps of the full Z-spectrum data to map magnetization transfer ratio asymmetry (MTR_{asym}). For pre-processing, we included co-registration between the three-dimensional (3D) T1-weighted (T1W) and full Z-spectrum images, brain-tissue segmentation of the 3D T1W image, and spatial normalization of the co-registered full Z-spectrum images. In the normalized full Z-spectrum images, the cerebrospinal fluid (CSF) signals were masked. The MTR_{asym} maps were calculated after B_0 correction. Finally, statistical analyses were performed to compare the MTRasym maps obtained with and without masking the CSF signals. MNI, Montreal Neurological Institute; WM, white matter; GM, gray matter.

matter because voxels with more than 50% CSF are usually of no interest in some clinical evaluations. After this pre-processing step, we obtained the MTR_{asym} map, which is the CEST asymmetry map.

4. Mapping of MTR_{asym} from full Z-spectrum data

We created two sets of MTR_{asym} maps for each offset frequency for each subject using the pre-processed full Z-spectrum data in the masked and unmasked conditions by employing the following steps. The spatially normalized full Z-spectrum images in the masked and unmasked conditions were divided by the reference image S_0 obtained at an offset frequency of –40 ppm. To determine the offset frequency for the minimum signal, the B_0 inhomogeneity correction step was performed using the 10th degree polynomial fitting,[15] assuming that the actual water resonance was at the frequency with the lowest signal intensity and excluding the fat-dominate voxels. The water resonance frequency was estimated as the frequency with the lowest signal intensity from the fitted curve and shifted along the direction of the offset axis to 0 ppm at its lowest intensity on a voxel-by-voxel basis. The MTR_{asym} maps with respect to the water frequency under the masked and unmasked conditions were obtained using the following equation:[3,16]

$$\mathrm{MTR}_{\mathrm{asym}} = \frac{S_{sat}(-\Delta\omega) - S_{sat}(+\Delta\omega)}{S_0} \quad (1)$$

Here, $\Delta\omega$ is the frequency difference with respect to water, S_{sat} is the signal with the saturation pulse, and S_0 is the signal observed without any saturation pulse. Usually, the CEST effect from the solute protons is detected at a frequency lower than 6 ppm with respect to water. We used the MTR_{asym} maps obtained at 0.86, 2.14, 3.00, and 3.43 ppm for the 3D-segmented gradient-echo EPI data and those obtained at 1, 2, 3.0, and 3.5 ppm for the 3D GRASE data.

5. Statistical analyses of MTR_{asym} maps

The MTR_{asym} maps obtained in the masked and unmasked conditions for each subject were smoothed using a Gaussian smoothing kernel at a full-width half maximum

of 8×8×8 mm^3. We compared the MTR_{asym} maps obtained in the masked and unmasked conditions using voxel-based and region-of-interest (ROI)-based methods. For the voxel-based analysis, the MTR_{asym} value in each voxel was compared between the masked and unmasked conditions using paired t-tests for each offset frequency and for each sequence, separately. A significance level of P=0.001 was applied without correcting for multiple comparisons in clusters with at least 30 contiguous voxels. This voxel-wise analysis was performed to define the ROIs in the brain.

The ROIs were defined at Brodmann area (BA) 10, BA21, cerebellar tonsil, declive, precuneus, and thalamus based on the results of the voxel-based analysis using the WFU PickAtlas toolbox (http://fmri.wfubmc.edu/software/pickatlas) (Radiology Informatics and Imaging Laboratory, Winston-Salem, NC, USA). BA10 is the anterior portion of the prefrontal cortex in the human brain, which includes the frontopolar, rostrolateral, and anterior prefrontal cortexes. BA21 is the part of the middle temporal gyrus. The ventricles were not selected as ROIs because many of the CSF signals in the ventricles were masked; hence, the differences in the ventricles were natural. The MTR_{asym} values for each ROI and at the four offset frequencies were obtained using the MarsBaR toolbox (http://marsbar.sourceforge.net/). The normal distribution of the MTR_{asym} values for each ROI was tested using the Kolmogorov-Smirnov

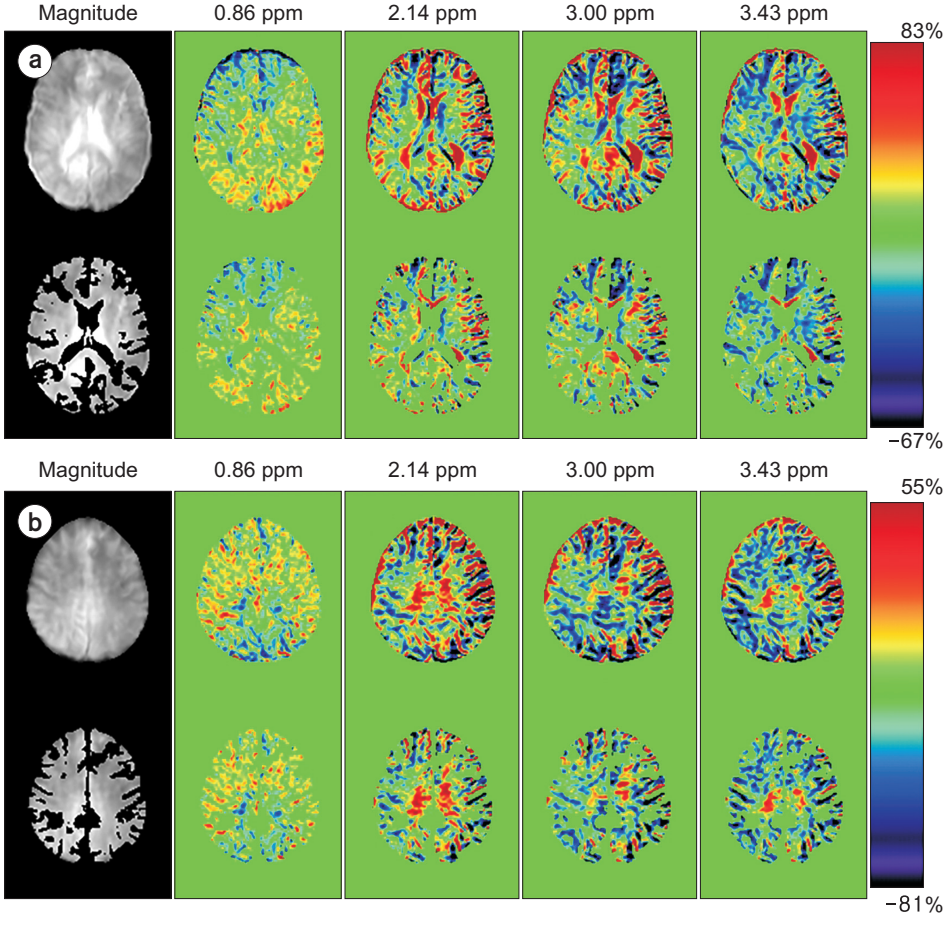

Fig. 2. Representative magnetization transfer ratio asymmetry (MTR_{asym}) maps acquired at four different offset frequencies and the corresponding reference image obtained without (top) and with (bottom) masking the cerebrospinal fluid (CSF) signals of the ventricle (a) and cortex levels (b) with the three-dimentional-segmented gradient-echo echo-planar imaging sequence. The MTR_{asym} maps were obtained at the offset frequencies 0.86, 2.14, 3.00, and 3.43 ppm. In the MTR_{asym} map, the color bar indicates the MTR_{asym} value in percentage. The MTR_{asym} values for the ventricle and perivascular space area were higher under the unmasked condition than that under masked condition. The MTR_{asym} values for the ventricles and around the ventricles were higher under the unmasked condition than that under the masked CSF signals.

method. Paired t-tests were used to compare the MTR_{asym} values between the masked and unmasked conditions for each ROI and each offset frequency. The results were regarded as significant if the two-tailed probability of the results was lower than 0.05. MedCalc (MedCalc Software, Ostend, Belgium) was used for the statistical analysis.

Results

Fig. 2 shows the representative MTR_{asym} maps acquired at four offset frequencies with the 3D-segmented gradient-echo EPI sequence. Fig. 3 shows the ones with the 3D GRASE sequence from the levels of the ventricle and cortex in the brain. Overall, the MTR_{asym} values were higher in the unmasked condition than in the masked condition, particularly for the periventricular white matter, areas near the perivascular space, and the ventricle. In addition, the MTR_{asym} map obtained with the 3D GRASE sequence seems to be overestimated compared with that obtained with the 3D-segmented gradient-echo EPI sequence.

1. Voxel-based analysis

In the 3D-segmented gradient-echo EPI sequence, the MTR_{asym} values in the unmasked condition were higher than those in the masked condition at offset frequencies of 0.86 ppm and 2.14 ppm (Supplementary Fig.1). However, the MTR_{asym} values in the unmasked condition were higher or lower than those in the masked condition at 3 ppm and 3.43 ppm frequencies as listed in Supplementary Table 1,

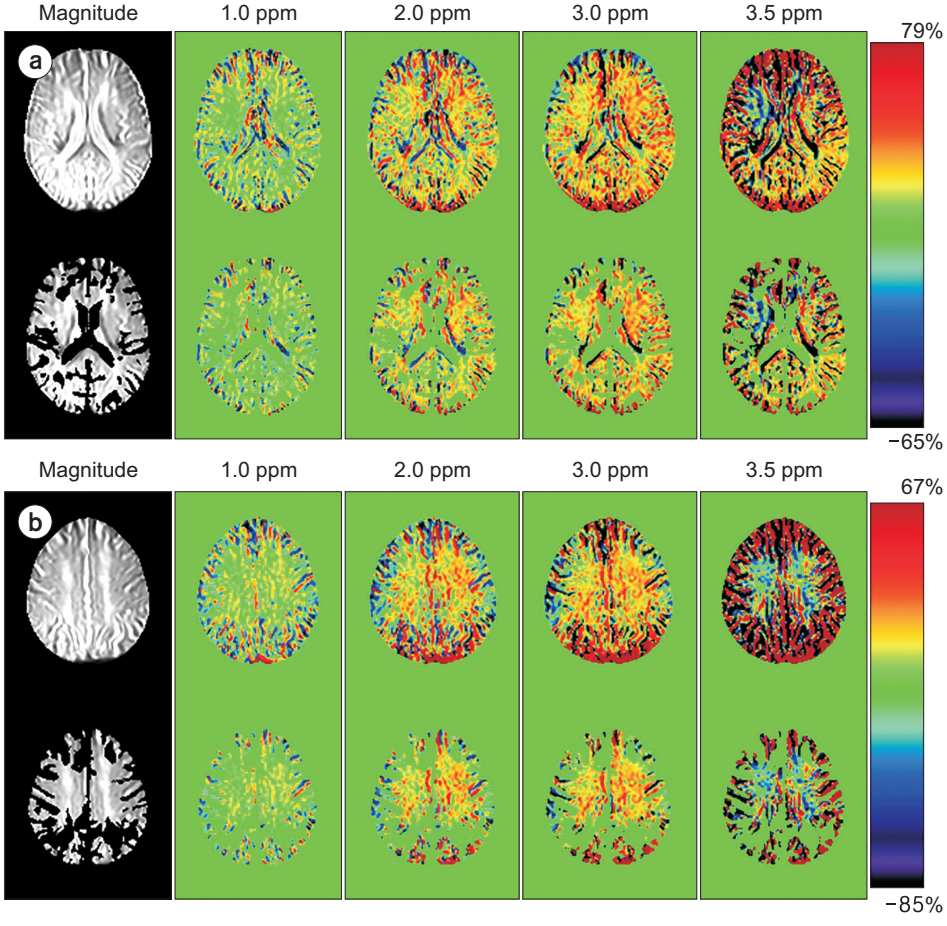

Fig. 3. Representative magnetization transfer ratio asymmetry (MTR_{asym}) maps at acquired at four different offset frequencies and the corresponding reference image obtained without (top) and with (bottom) masking the cerebrospinal fluid (CSF) signals at the ventricle (a) and cortex levels (b) with the three-dimentional gradient and spin-echo sequence. The MTR_{asym} maps were obtained at offset frequencies of 1.0, 2.0, 3.0, and 3.5 ppm. In the MTR_{asym} map, the color bar indicates the MTR_{asym} value in percentage. In general, the MTR_{asym} values for the areas of the brain were higher without masking the CSF signals (unmasked condition) than that with masking (masked condition).

which summarizes the result of the voxel-based comparisons of the MTR_{asym} maps between the masked and unmasked conditions in the 3D-segmented gradient-echo EPI sequence.

For the 3D GRASE sequence, only a few areas showed significant differences in the MTR_{asym} values between the two conditions. The MTR_{asym} values were greater in the unmasked condition than in the masked condition for the right inferior semi-lunar lobule (Talairach coordinates=1.13, –58.93, and –36.42; cluster size=66; Z-score=3.29) at an offset frequency of 2.14 ppm offset frequency and for the left precuneus (Talairach coordinates=0.32, –64.94, and 25.16; cluster size=434; Z-score=3.89) at an offset frequency of 3.00 ppm. No significant differences were observed in the MTR_{asym} values between the two conditions at other offset frequencies. Finally, all areas showed lower MT_{Rasym} values in the masked condition than in the unmasked condition.

2. ROI-based analysis

Table 2 summarizes the results of the ROI-based comparisons of the MTR_{asym} values between the masked and unmasked conditions for each ROI and for each offset frequency obtained with the 3D-segmented gradient-echo EPI sequence. The MTR_{asym} values were higher in the unmasked condition than in the masked condition at offset frequencies of 0.86, 2.14, 3.00, and 3.43 ppm. The MTR_{asym} values were significantly different between the masked and unmasked conditions for the following brain regions: BA21, tonsil, and declive at 0.86 ppm; tonsil and thalamus at 2.14 ppm, indicating the presence of guanidium protons; BA10 and BA21 at 3.00 ppm, indicating the presence of amines; and BA10, BA21, and precuneus at 3.43 ppm.

Table 2. Results of ROI-based analyses of MTR_{asym} values (percent) obtained from a 3D-segmented gradient-echo EPI sequence

ppm	ROI	Masked	Unmasked	*P*-value
0.86 (Hydroxyl)	BA10	–0.238±0.424	–0.423±0.777	0.168
	BA21	0.452±0.279	0.701±0.411	0.005
	Tonsil	0.389±0.503	0.771±0.805	0.006
	Declive	0.605±0.314	1.033±0.531	0.001
	Precuneus	–0.100±0.170	–0.356±0.545	0.064
	Thalamus	0.003±0.472	0.042±0.078	0.783
2.14 (Guanidium)	BA10	–0.247±0.380	–0.403±0.858	0.416
	BA21	0.072±0.418	0.052±0.687	0.832
	Tonsil	0.531±0.683	0.742±0.904	0.050
	Declive	0.264±0.389	0.309±0.762	0.754
	Precuneus	–0.013±0.118	0.077±0.437	0.422
	Thalamus	0.459±0.753	0.774±1.124	0.038
3.00 (Amine)	BA10	–0.742±0.530	–1.169±0.915	0.025
	BA21	–0.489±0.462	–0.761±0.757	0.025
	Tonsil	–0.346±1.153	–0.372±1.770	0.902
	Declive	–0.316±0.438	–0.539±0.914	0.234
	Precuneus	–0.091±0.158	–0.169±0.488	0.486
	Thalamus	–0.557±1.046	–0.622±1.280	0.472
3.43 (Amide)	BA10	–0.955±0.703	–1.622±1.229	0.011
	BA21	–0.645±0.417	–1.069±0.664	0.001
	Tonsil	–0.253±0.537	–0.262±0.873	0.947
	Declive	–0.407±0.465	–0.695±1.193	0.302
	Precuneus	–0.171±0.125	–0.385±0.350	0.021
	Thalamus	–0.572±0.775	–0.638±0.987	0.520

Negative numbers indicate higher signals at the negative offset frequency. Data are presented as mean±standard deviation.
ROI, region-of-interest; MTR_{asym}, magnetization transfer ratio asymmetry; 3D, three-dimentional; EPI, echo-planar imaging; BA, Brodmann area.

Table 3. Results of ROI-based analyses of MTR_{asym} values (percent) obtained from a 3D GRASE sequence

ppm	ROI	Masked	Unmasked	*P*-value
1.0 (Hydroxyl)	BA10	−0.162±0.301	−0.336±0.443	0.026
	BA21	0.088±0.138	0.152±0.199	0.028
	Tonsil	0.339±0.298	0.451±0.394	0.025
	Declive	0.082±0.148	0.178±0.181	0.006
	Precuneus	−0.037±0.099	−0.027±0.251	0.858
	Thalamus	−0.140±0.390	−0.326±0.552	0.013
2.0 (Guanidium)	BA10	0.425±1.079	0.483±1.500	0.729
	BA21	0.610±0.361	0.985±0.523	0.0002
	Tonsil	1.387±0.629	1.922±0.894	0.001
	Declive	0.599±0.443	0.998±0.599	0.003
	Precuneus	0.140±0.254	0.551±0.611	0.011
	Thalamus	0.603±0.591	0.774±0.836	0.123
3.0 (Amine)	BA10	−0.531±1.344	−1.232±1.973	0.022
	BA21	−0.603±0.383	0.916±0.646	0.010
	Tonsil	1.738±0.542	2.423±0.824	0.001
	Declive	0.758±0.416	1.359±0.480	0.0002
	Precuneus	0.281±0.305	1.017±0.740	0.001
	Thalamus	0.505±1.038	0.622±1.364	0.338
3.5 (Amide)	BA10	−2.071±1.711	−3.604±2.566	0.001
	BA21	0.140±0.660	0.253±0.989	0.336
	Tonsil	2.048±1.060	2.840±1.463	0.003
	Declive	0.253±0.572	0.713±0.511	0.004
	Precuneus	0.198±0.313	0.891±0.643	0.0003
	Thalamus	−0.241±1.723	−0.405±2.519	0.556

Negative numbers indicate higher signals at the negative offset frequency. Data are presented as mean±standard deviation.
ROI, region-of-interest; MTR_{asym}, magnetization transfer ratio asymmetry; 3D, three-dimentional; GRASE, gradient and spin-echo; BA, Brodmann Area.

Table 3 summarizes the results of the ROI-based comparisons of the MTR_{asym} values between the masked and unmasked conditions for each ROI and for each offset frequency obtained with the 3D GRASE sequence. Significant differences in the MTR_{asym} values between the two conditions were observed for the following brain areas: all ROIs except the precuneus at 1.0 ppm, indicating the presence of hydroxyl protons; all ROIs except BA10 and thalamus at 2.0 ppm; all ROIs except thalamus at 3.0 ppm; and all ROIs except BA21 and thalamus at 3.5 ppm, indicating the presence of amides.

Discussion

The perivascular space widens with the loss of brain-tissue. We investigated the MTR_{asym} values in elderly subjects after masking the CSF signals in the brain. The MTR_{asym} values for certain brain areas were significantly different between the masked and unmasked conditions at the amide and amine offset frequencies. The difference depended on the sequence type used.

1. CSF signals affect MTR_{asym} values

We found significant contributions of the CSF signals to the MTR_{asym} map, which overestimated the MTR_{asym} values in the elderly human brain. The MTR_{asym} values were altered with the masking of the CSF signals, irrespective of the saturation offset frequency with respect to water. In elderly subjects, the overestimation of the MTR_{asym} values due to the changes in the CSF signals could be attributed to brain atrophy, which results in widening of the perivascular spaces, which are basically CSF spaces. To obtain accurate CEST effects in the elderly brain, the CSF signal should

be masked either using some post-processing technique or using some data acquisition method, e.g., an inversion-recovery preparation. This corrected MTR_{asym} value might be valuable for evaluating brain metabolites in patients with neurodegenerative diseases.[17,18] For the amide and amine protons, the results of the ROI-based analyses showed that the MTR_{asym} values for the thalamus were not significantly different between the two conditions for both the sequences, whereas the values were significantly different for the precuneus. Several previous studies have reported brain atrophy at the precuneus in elderly subjects, but not at the thalamus.[11] Our result, therefore, showed that the difference in the MTR_{asym} values between the two conditions could be related to CSF contributions in the CEST signals rather than to an artifact. Some regions showed a difference in the MTR_{asym} values between the unmasked and masked conditions only at the hydroxyl offset frequency. This indicates that it is difficult to accurately measure the MTR_{asym} value at this offset frequency using a 3T MRI system because of the proximity to water.

2. CSF contribution to MTR_{asym} value depends on the acquired sequence type

The MTR_{asym} values acquired using the two sequences were sensitive to the contribution of the CSF signals. For the 3D-segmented gradient-echo EPI sequence, we used a relatively lower power saturation pulse than that used for the 3D GRASE sequence. At the amide offset frequency, the MTR_{asym} values were significantly different between the two conditions for BA10, BA21, and precuneus in the case of the EPI sequence, but for BA10, tonsil, declive, and precuneus in the case of the GRASE sequence. At the amine offset frequency, the MTR_{asym} values were significantly different between the two conditions only for BA10 and BA21 with the EPI sequence, but at all the ROIs except the thalamus with the GRASE sequence. These differences could be attributed to the fact that the 3D GRASE sequence more strongly reflects the effect of the CSF signal than the 3D EPI sequence. The GRASE sequence is used in multiple spin-echo pulses. Another probable reason more ROIs showed significant differences between the masked and unmasked conditions in the GRASE sequence than they did in the segmented EPI sequence would be the quality of the full Z-spectrum. The full Z-spectrum with the 3D GRASE sequence was much broader than that with the 3D EPI sequence. It may be necessary to evaluate the MTR_{asym} value using a relatively low B_1 power of the saturation pulse for the 3D GRASE sequence, which may slightly increase the sharpness of the full Z-spectrum; however, a previous study showed that the full Z-spectrum with a B_1 amplitude of 1 μT was still broad.[19] When using a low B_1 power, the effect of the contribution of CSF signals to the MTR_{asym} value may therefore be similar to that in this study. Nevertheless, further studies with different types of pulse sequences should be performed to validate these findings.

3. Study limitations

First, we only evaluated the full Z-spectrum data acquired using a pulsed-saturation RF preparation.[20,21] Because saturation with a continuous-wave RF pulse is more effective than that with the pulse-wave RF, the effect of CSF signals on the full Z-spectrum data needs to be evaluated. However, a continuous-wave RF pulse for saturation cannot be generated on most clinical scanners owing to hardware limitations. Second, in this study, the B_1 amplitude was not optimized for amide protons or amine because we did not target one specific proton. The saturation preparation depends only on the B_1 amplitude and saturation duration. A low power is recommended for the saturation of amide protons, but a relatively high power is recommended for the saturation of amine protons. For the 3D GRASE sequence, the B_1 power for the saturation transfer may have been too high because the full Z-spectrum obtained was broad. Third, the B_0 correction method using the 10th degree polynomial fitting may not be optimal. Each voxel has a small difference in precession frequency due to structural susceptibility, which is particularly significant at high magnetic fields.[5] B_0 inhomogeneity leads to a shift in the water resonance frequency, resulting in direct asymmetric water saturation effects, and thus, artificial CEST effects in an asymmetry analysis. A better method may have to be applied for correcting the B_0 inhomogeneity.[4,15] Fourth, we used the MTR_{asym} maps obtained at 0.86, 2.14, 3.00, and 3.43 ppm for the 3D-segmented gradient-echo EPI data and

those obtained at 1, 2, 3.0, and 3.5 ppm for the 3D GRASE data. The slight differences in the offset frequencies in the two sequences may not represent the same exchangeable protons for both measurements. In this study, we did not focus on evaluating the interpretation method after field inhomogeneity correction. Finally, we included a relatively small population in this study. Further large-scale studies should be conducted to validate our observations.

Conclusions

Depending on the sequence type, the MTR_{asym} values can be overestimated for some areas of the elderly human brain if CSF signals are unmasked. Therefore, to obtain accurate MTR_{asym} values in elderly subjects, it is necessary to apply method to minimize the contribution of CSF signals on the full Z-spectrum. In other words, the increased MTR_{asym} values in the case of Alzheimer's disease due to increased CSF signal intensity can be used as an imaging biomarker.

Acknowledgements

This study was supported by the National Research Foundation of Korea (NRF) grant funded by the Korea government (MSIP) (2014R1A2A2A01002728), the Basic Science Research Program through the National Research Foundation of Korea (NRF) funded by the Ministry of Education (2016R1D1A1B03930720), and the Convergence of Conventional Medicine and Traditional Korean Medicine R&D program funded by the Ministry of Health & Welfare through the Korea Health Industry Development Institute (KHIDI) (HI16C2352).

Conflicts of Interest

The authors have nothing to disclose.

Availability of Data and Materials

All relevant data are within the paper and its Supporting Information files.

Ethics Approval and Consent to Participate

The study was approved by the Institutional Review Board of Kyung Hee University Hospital at Gangdong (IRB approval number; 2015-02-006-001).

References

1. Oh JH, Kim HG, Woo DC, Jeong HK, Lee SY, Jahng GH. Chemical-exchange-saturation-transfer magnetic resonance imaging to map gamma-aminobutyric acid, glutamate, myoinositol, glycine, and asparagine: phantom experiments. J Korean Phys Soc. 2017;70:545-553.
2. Dagher AP, Aletras A, Choyke P, Balaban RS. Imaging of urea using chemical exchange-dependent saturation transfer at 1.5T. J Magn Reson Imaging. 2000;12:745-748.
3. Guivel-Scharen V, Sinnwell T, Wolff SD, Balaban RS. Detection of proton chemical exchange between metabolites and water in biological tissues. J Magn Reson. 1998;133:36-45.
4. Zhou J, Lal B, Wilson DA, Laterra J, van Zijl PC. Amide proton transfer (APT) contrast for imaging of brain tumors. Magn Reson Med. 2003;50:1120-1126.
5. van Zijl PC, Yadav NN. Chemical exchange saturation transfer (CEST): what is in a name and what isn't? Magn Reson Med. 2011;65:927-948.
6. Bryant RG. The dynamics of water-protein interactions. Annu Rev Biophys Biomol Struct. 1996;25:29-53.
7. Ward KM, Aletras AH, Balaban RS. A new class of contrast agents for MRI based on proton chemical exchange dependent saturation transfer (CEST). J Magn Reson. 2000;143:79-87.
8. Xiao Y, Ma B, McElheny D, Parthasarathy S, Long F, Hoshi M, et al. Aβ(1-42) fibril structure illuminates self-recognition and replication of amyloid in Alzheimer's disease. Nat Struct Mol Biol. 2015;22:499-505.
9. Zhang Y, Man VH, Roland C, Sagui C. Amyloid properties of asparagine and glutamine in prion-like proteins. ACS Chem Neurosci. 2016;7:576-587.
10. Haris M, Cai K, Singh A, Hariharan H, Reddy R. In vivo mapping of brain myo-inositol. Neuroimage. 2011;54:2079-2085.
11. Jahng GH, Lee DK, Lee JM, Rhee HY, Ryu CW. Double in-

version recovery imaging improves the evaluation of gray matter volume losses in patients with Alzheimer's disease and mild cognitive impairment. Brain Imaging Behav. 2016;10:1015-1028.
12. Tohka J. Partial volume effect modeling for segmentation and tissue classification of brain magnetic resonance images: a review. World J Radiol. 2014;6:855-864.
13. Sun PZ, Lu J, Wu Y, Xiao G, Wu R. Evaluation of the dependence of CEST-EPI measurement on repetition time, RF irradiation duty cycle and imaging flip angle for enhanced pH sensitivity. Phys Med Biol. 2013;58:N229-N240.
14. Zhu H, Jones CK, van Zijl PC, Barker PB, Zhou J. Fast 3D chemical exchange saturation transfer (CEST) imaging of the human brain. Magn Reson Med. 2010;64:638-644.
15. Kim M, Gillen J, Landman BA, Zhou J, van Zijl PC. Water saturation shift referencing (WASSR) for chemical exchange saturation transfer (CEST) experiments. Magn Reson Med. 2009;61:1441-1450.
16. Zaiss M, Xu J, Goerke S, Khan IS, Singer RJ, Gore JC, et al. Inverse Z-spectrum analysis for spillover-, MT-, and T1 -corrected steady-state pulsed CEST-MRI — application to pH-weighted MRI of acute stroke. NMR Biomed. 2014;27: 240-252.
17. Tietze A, Blicher J, Mikkelsen IK, Østergaard L, Strother MK, Smith SA, et al. Assessment of ischemic penumbra in patients with hyperacute stroke using amide proton transfer (APT) chemical exchange saturation transfer (CEST) MRI. NMR Biomed. 2014;27:163-174.
18. Zhou J, Blakeley JO, Hua J, Kim M, Laterra J, Pomper MG, et al. Practical data acquisition method for human brain tumor amide proton transfer (APT) imaging. Magn Reson Med. 2008;60:842-849.
19. Sun PZ, Farrar CT, Sorensen AG. Correction for artifacts induced by B(0) and B(1) field inhomogeneities in pH-sensitive chemical exchange saturation transfer (CEST) imaging. Magn Reson Med. 2007;58:1207-1215.
20. Zu Z, Li K, Janve VA, Does MD, Gochberg DF. Optimizing pulsed-chemical exchange saturation transfer imaging sequences. Magn Reson Med. 2011;66:1100-1108.
21. Tee YK, Khrapitchev AA, Sibson NR, Payne SJ, Chappell MA. Evaluating the use of a continuous approximation for model-based quantification of pulsed chemical exchange saturation transfer (CEST). J Magn Reson. 2012;222:88-95.